

# Free-Standing All-Nanoparticle Thin Fibers: A Novel Nanostructure Bridging Zero- and One-Dimensional Nanoscale Features

By Jia Yan, Ziguang Chen, Jinyue Jiang, Li Tan,\* and Xiao Cheng Zeng

Nanoscience and nanotechnology have had great success in revealing nanostructures with unique dimensionalities. To highlight a few, nacre is composed of nanolayers of inorganic crystallites and biopolymers<sup>[1]</sup> and is therefore 2D in nature and exhibits extraordinary toughness.<sup>[2,3]</sup> Derivatives of such a structure can be utilized to suit a variety of engineering applications due to their fine structure. Nanotubes, nanobelts, or nanofibers all possess a 1D structure, where the long dimension promotes applications for advanced functional materials and the short dimension delivers superior electronic, mechanical, or electromechanical properties. Long-lasting impacts of these 1D features are being generated in multiple fields. For example, nanotubes could be used as scanning probes to provide unprecedented resolution to scanning probe microscopy,<sup>[4,5]</sup> continuous nanofibers can be efficient intermediate layers in nanocomposites,<sup>[6,7]</sup> and functional nanobelts demonstrating an electromechanical coupling effect can be potential candidates to power future nanosystems.<sup>[8–10]</sup> While nanoparticles or nanodots qualify as 0D structures and also have peculiar electronic or optoelectronic properties, their role as building blocks for higher-order subjects is one of their most prominent features. Demonstrated examples include packed particle films for high sensitivity detection,<sup>[11]</sup> fabricated arrays for photonic crystals,<sup>[12–14]</sup> and layered pores for energy storage.<sup>[15,16]</sup> More interestingly, it is even possible to form laminates of nanolayers with a carefully designed manufacturing and surface chemistry approach, rendering the formation of artificial nacre.<sup>[17,18]</sup> Properties of resulting assemblies usually exceed that of individual nanoparticles, where a large surface-to-volume ratio is believed to be one of the reasons for such a collective effect.

With so much evidence for the structural flexibility of nanoparticles, stumbling blocks still impede the control of the

growth of these 0D elements into a 1D assembly. Major barriers to unidirectional growth are difficulties to attenuate the robust interactions between nanoparticles and their isotropic shape. Patterned templates or surfaces could guide the growth of these building blocks.<sup>[19–27]</sup> An anisotropic surface treatment atop nanoparticles could regulate their assembly to a certain degree.<sup>[28,29]</sup> Free-standing strings of nanoparticles are rarely observed. A good strategy to devise a high throughput manufacturing of these assemblies with decent uniformity and a large aspect ratio has not been reported.

We present our strategy in this communication to make unidirectionally grown and template-free, i.e., free-standing, 1D nanostructures by using uniform nanoparticles. We call this newly discovered structure a particle-fiber, implying the 0D nature of the building blocks. These string-like structures are grouped into forests after fabrication and have a few unique features, such as a high aspect ratio (length vs. diameter  $\geq 2500$ ), a uniform profile (diameter of 1.5  $\mu\text{m}$ ), and a relatively strong mechanical strength. Since these 1D assemblies have many gaps between the building blocks, chemical vapor deposition (CVD) can be utilized to further reinforce these novel nanostructures.

The principle of our strategy is to take advantage of the unidirectional growth of ice<sup>[18,30,31]</sup> and its easy removal during a subsequent freeze-drying process. The key elements of our methodology are shown schematically in Figure 1a–c. An aqueous suspension of polymeric nanoparticles is filled in a cold finger (Fig. 1a, left), which is designed to have one side particularly sensitive to a temperature change and all other sides insulated from the cold source. Then, we load the suspension and the finger into an alcohol bath exposed over a vapor of liquid nitrogen (Fig. 1a, middle). Since the sensitive side of the cold finger faces downward in the bath, water in the suspension freezes in an upward, unidirectional fashion by forming ice crystals. Since ice forms by expelling all other ingredients previously dispersed, many gaps will form either inside<sup>[18]</sup> or between<sup>[31]</sup> the ice nuclei. Since these gaps also grow in a predetermined unidirectional fashion, free-standing forests of 1D string-like features form after all the nanoparticles fall into these gaps (Fig. 1a, right).

Scanning electron microscope (SEM) images of fabricated particle-fibers are shown in Figures 1b–f. The main bodies of forests (Fig. 1b) have a thickness of 4.0 mm and are fibrous in texture. Figure 1c shows a zoomed-in image of the bundles, where a uniform diameter is evident. Figures 1d and e reveal two

[\*] Prof. L. Tan, Dr. J. Yan, Z. Chen, Dr. J. Jiang  
Department of Engineering Mechanics and Nebraska Center for  
Materials and Nanoscience  
University of Nebraska  
Lincoln, NE, 68588 (USA)  
E-mail: ltan4@unl.edu  
Prof. X. C. Zeng  
Department of Chemistry  
University of Nebraska  
Lincoln, NE, 68588 (USA)

DOI: 10.1002/adma.200801130

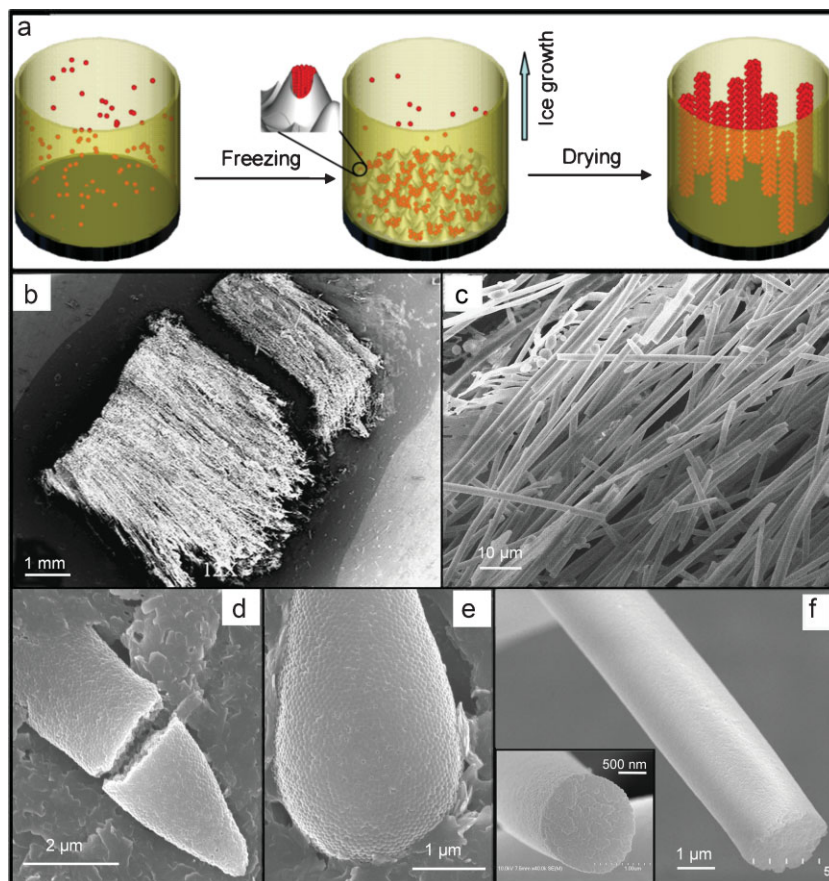


**Figure 1.** a) Schematic illustration of the formation of all-nanoparticle thin fibers, where an aqueous suspension of polymer nanoparticles is poured into a cold finger (left), frozen in an alcohol bath exposed to a vapor of liquid nitrogen (middle), and then freeze dried to remove the ice crystals by leaving a relief of free-standing forests of particle-fibers. Note that nanoparticles fall into gaps inside or between ice nuclei to initiate the growth of fibers. b–f) SEM images of the fabricated fibers, where (b) shows a bundle of these structures with a length of 4.0 mm, (c) is a zoomed-in image of the unidirectionally grown fiber, (d) and (e) show two types of starting points of the fiber, and (f) presents a long stem of a fiber with a smooth and rounded profile. The cross-section of the fiber is shown in inset of (f), where terraces of nanoparticles are clearly visible and the measured diameter of the nanostructure is 1.5  $\mu\text{m}$ . Note that above fibers are laid down to increase contact with the conducting sample holder for better imaging under SEM.

distinctive features of the starting points of fibers, where one has a sharp pointy feature (Fig. 1d) and the other one is quite dull (Fig. 1e). While both of them are completely comprised by small nanoparticles, they are negative reliefs of the gaps inside<sup>[18]</sup> or between<sup>[31]</sup> the ice nuclei. Certainly, this discovery validates their initial concave shapes as sketched in Figure 1a. In addition, we found that the lengths of both features are quite short (2.0–4.0  $\mu\text{m}$ ) compared to the long stems of fibers seen in Figure 1c, indicating a short time frame ( $\sim 0.1$ – $0.2$  s) to initiate the fiber growth in a unidirectional fashion. The final stems of particle-fibers (Fig. 1f) exhibit a rather smooth and circular outer surface. The inset in Figure 1f further shows layered terraces in the cross-section of one fiber, suggesting a close packed motif for these nanoparticles. Since the measured diameter of the fiber is 1.5  $\mu\text{m}$ , the estimated aspect ratio (length vs. diameter) for this novel nanostructure is more than 2500.

While the fabrication system is simple, the role of surface tension from the nanoparticles is worth expounding upon. The polymeric nanoparticles have a polystyrene core and a monolayer of surfactant physisorbed over the shell. This thin layer stabilizes the hydrophobic nanoparticles in water and gives rise to a uniform aqueous dispersion. While it is not surprising to see uniform features fabricated from this simple system, it is quite unusual to find the final structures with a rounded cross-section. One of the possibilities leading to such a structure lies in the comparatively poor low-temperature stability of surfactants,<sup>[32]</sup> where nanoparticles easily aggregate to form round bundles.<sup>[33,34]</sup> We also noticed that a palette-like relief is revealed by replacing these hydrophobic nanoparticles with hydrophilic powders<sup>[35a]</sup> or particles<sup>[35b]</sup> after the freeze-drying process. All of these suggest that surface tension is an important aspect, supporting some of the theoretical discussions.<sup>[31,35a]</sup> Certainly, an alteration of the size of these hydrophobic nanoparticles could also affect the surface tension, resulting in different morphologies after the final assembly. This complex interplay of size to the fabrication is under investigation and the results will be published elsewhere.

Even though high pressure, up to 200 MPa, can be created as the water freezes in a sealed environment, the frozen water in this case has no tendency to expand along the hoop directions of particle-fibers as one of the axial surfaces is open to air. One may then expect that these stacked nanoparticles are full of defects or vacancies and cannot maintain their string-like structures after the ice template is removed, but experimental data suggests otherwise and thus we believe surface tension between these nanoparticles is still the major force.<sup>[25]</sup> Such a seemingly subtle interaction could group individual nanoparticles to form strong aggregates, where our estimated value of interactions can be more than 140 MPa.<sup>[36]</sup> Hence, collective interactions between many small particles render the final assembly a highly packed, defect-free structure. Figure 2a shows a transmission electron microscopy (TEM) image of such a particle-fiber, where the spherical shape of these nanoparticles suggests unnoticed deformation after the freezing process. It is worthwhile to note that in order to form nicely organized fibers, the kinetics of ice growth and particle aggregation must be delicately balanced. Parameters to synchronize these two processes include freezing rate, concentration of nanoparticles, and size of the nanoparticles. We observed that a variation of these parameters affects the morphology of the final nanostructures, which is beyond the scope of this report.

To fully appreciate the importance of surface interactions between nanoparticles, we provide a qualitative analysis for the

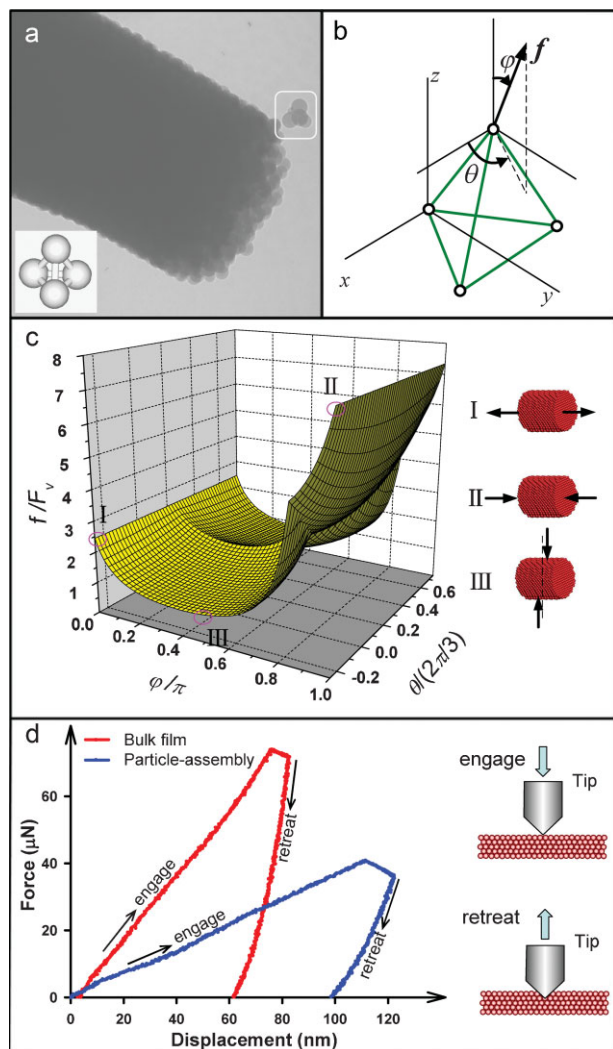


**Figure 2.** a) TEM image shows the spherical shape of individual nanoparticles and a tetragonal element of the particle-fiber. This element is used as a basic model (inset) to evaluate the strength of the porous fiber. b) Free-body diagram of the tetragonal element with an external load applied from the top. Joints and rigid bars represent the locations of the nanoparticles and the distances in between, respectively. c) Estimated minimum forces to destabilize the tetragonal element, where the magnitude of these forces varies depending upon load directions highlighted with purple circles. The legend shows the corresponding failure modes likely to happen for the particle-fiber. d) Load-displacement responses of thin films of particles or bulk polystyrene under nanoindentation. The legend shows a schematic of the setup.

mechanical properties of our particle-fibers. Since the nanoparticles are all grouped in a close-packed fashion as indicated by the TEM image in Figure 2a, we picked a tetragonal element (Fig. 2a, inset) to start this analysis. Particularly, three nanoparticles in this element occupy a single layer, with the fourth sitting atop of this layer. The free-body diagram is shown in Figure 2b, where the joints and rigid bars represent the locations of the nanoparticles and the distances in between, respectively. We now assign the long dimensional direction of the fiber as the z-axis and the bottom of the three nanoparticles as the x–y plane, with one of

them fixed at the origin of the coordinate. Next, we make two assumptions, i.e., the nanoparticles are rigid and they can rotate freely on the surfaces of neighboring particles. Since the van der Waals force between two neighboring particles is given by<sup>[37,38]</sup>

$$F_v = \frac{Ar}{12D^2}, \quad (1)$$

where  $A$  is the Hamaker constant (typically  $\sim 10^{-19}$  J) for van der Waals interactions exposed to air,  $r = d_p/2$  is the radius of the nanoparticles ( $d_p$  is the diameter of the nanoparticle), and  $D$  is the so-called atomic gap distance ( $\sim 3.0$  Å), we can assume nanoparticles will fall apart when the tensile force between them exceeds  $F_v$ . In our experiment, the estimated value of  $F_v$  is 3.7 nN when  $d_p$  is 80 nm. Using this rationale as a guide to stabilize our tetragonal element, each tensile force in the rigid bars resulting from an external impact  $f$  has to be smaller than  $F_v$ . We can then estimate the minimum force to destabilize this element as a function of directions

$$f = C(\varphi, \theta)F_v, \quad (2)$$

where  $C(\varphi, \theta)$  is the proportional ratio between  $f$  and  $F_v$ , and  $(\varphi, \theta)$  determines the direction of  $f$  in our coordinate (Fig. 2b). Since the free-body diagram is symmetric, we calculated the solutions for  $C(\varphi, \theta)$  in the range of  $0 \leq \varphi \leq \pi$  and  $-\frac{\pi}{6} \leq \theta \leq \frac{\pi}{2}$  only, and the results are shown in Figure 2c. Particularly, when  $\varphi = 0, \pi/2, \text{ or } \pi$ , the calculated external impact  $f$  will be equal to  $\sqrt{6}F_v, \frac{\sqrt{3}}{2}F_v, \text{ or } 3\sqrt{6}F_v$ , respectively, representing the minimal tensile, shear, or compression force to destabilize the tetragonal element. Finally, we can estimate the magnitude of a few critical stresses to break our fabricated fiber. We express the stress as  $\sigma = Nf/S$ , where  $S$  is the cross-sectional area of the nanostructure,  $N$  is the number of nanoparticles in a single layer, and  $f$  is the calculated minimal load force to impact the tetragonal element. When  $d_p$  is 80 nm, estimated critical tensile, compressive and shear stress to break the fiber are 1.64, 4.91, and 0.58 MPa, respectively. A small magnitude of the shear stress indicates the brittleness of the 1D structure, which further explains observed shearing off of the fiber along its hoop direction ( $\varphi = \pi/2$ ) as shown in Figure 1f.

One question yet unresolved is why these particle-fibers stand freely without collapsing. We address this concern from the angle of mechanical instability, or in other words, buckling. The critical or maximum value for unbuckled length of a slim structure under its own weight is<sup>[39,40]</sup>

$$l_{cr} = \left( \frac{7.837EI}{q} \right)^{1/3} \quad (3)$$

where  $I$  = area moment of inertia,  $q$  = gravity in unit length, and  $E$  = effective modulus of elasticity. The effective modulus of elasticity can be estimated either by condensing all the mass in the effective cross-section of the fiber,<sup>[41a]</sup> or using a delicate surface force model.<sup>[41b]</sup> An approximate value for a good stacking of nanoparticles without buckling is a few millimeters,<sup>[41]</sup> which qualitatively supports our experimental

observations. However, one might suspect these high-aspect ratio structures could potentially buckle under influences greater than gravity, for instance, capillary forces, electrostatic interactions, or even van der Waals forces. We have looked at this issue in other cases with array of nanobeams.<sup>[42]</sup> Forests of the beams indeed could buckle due to their interactions at a close distance ( $\sim 100$  nm). Our fabricated forests of fibers are spaced more than  $20 \mu\text{m}$  apart. Therefore, the possibility of a collective buckling can be safely excluded.

Nanoindentation was used to look at the mechanical deformations of the particle assemblies. Two samples were prepared: one is a solid bulk film of polystyrene and the other is a close-packed thin layer of polystyrene nanoparticles. The selection of a layered assembly as opposed to the particle-fiber avoids possible slipping or rolling of the fibers during nanoindentation and allows the collection of information on mechanical strength or modulus of the assembly rather easily. The bulk film serves as a reference for interpretation. In Figure 2d, the force is applied in parallel to the surface normal of either sample by a sharp tip and the load increases when the tip engages toward the layer. When the tip is retreated against the layer, an unloading curve is obtained. Both the slopes on the engage and retreat curves are relevant to the mechanical strength of the specimen. It is clear that the particle-assembly deforms much easier than the solid film. Particularly, the slopes of the engage and retreat curves are 0.36 and 2.36 for the particle-assembly, respectively, while for the bulk film, they are 1.19 and 6.02. Since the slope determines the modulus of a material, our results suggest that the modulus of the particle-assembly is about one third of the bulk polystyrene, qualitatively matching the estimated strength.<sup>[41]</sup> Moreover, it is also apparent that after indentation the permanent deformation of the particle-assembly is much larger than the bulk film, indicating the porous nature of the assembly (Fig. 2d).

The porous nature of particle-fibers affords many opportunities for further enrichment. One example is mechanical reinforcement. A variety of techniques can be used for this, including thermal annealing, CVD, or backfilling with resin after drying. We use the CVD route as a versatile example since there is no need to break the vacuum after the ice removal and a variety of chemicals can be incorporated. CVD is handled by injecting drops of reactive chemicals into the freeze-drying chamber after the ice in the porous structure is removed. In particular, we found silane molecules are effective to adsorb over our fibers since the surfaces of the particles are partially hydrophilic after the brief vacuum pumping. Adsorbed silanes easily reacted with surface water to form siloxane networks between neighboring molecules, resulting in a firm cover over the 1D assemblies. Figures 3a–c illustrate a photograph of the cake-like forests (Fig. 3a) and two TEM images (Figs. 3b and c). The cake-like forests kept their structure integrity even after drastic maneuvers were performed on the sample. The main bodies of forests (Fig. 3a) have a thickness of more than 3.0 mm and are shiny, white and fibrous, where opaque-looking suggests organized packing of fine particles. Final TEM imaging was acquired after transferring the fiber by spreading a small chunk of cake over a TEM grid with ethyl alcohol. Figure 3b shows such a fiber after CVD, where no appreciable change in diameter is observed. Figure 3c shows a

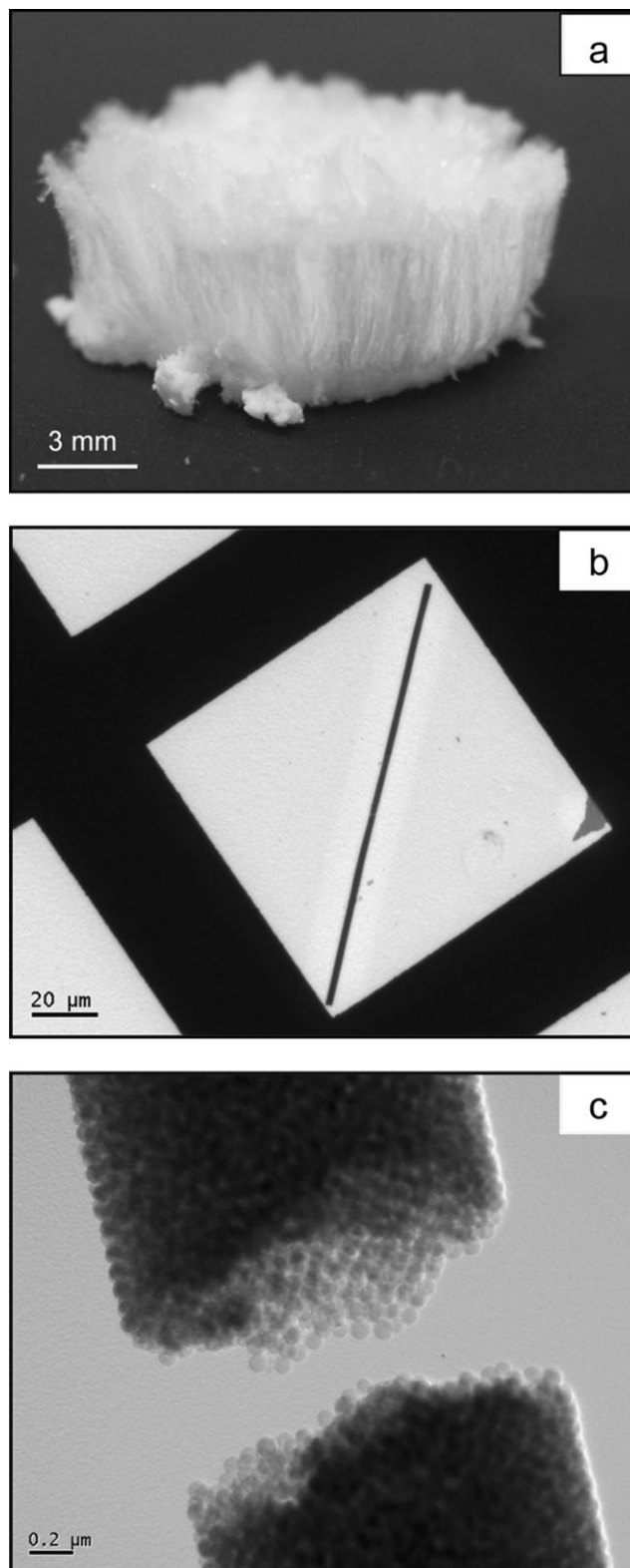


**Figure 3.** a) A photographic image of a cake-like forest reinforced after CVD. b) TEM image of a long particle-fiber ( $\sim 100 \mu\text{m}$ ), which was spread over a copper grid. c) A zoomed-in TEM image of a ruptured section of this particle-fiber, where complex topography indicates the ductile nature of this 1D assembly.

zoomed-in image of a broken fiber. A thin layer of coating is clearly visible between neighboring nanoparticles and complex topography of the ruptured surfaces suggests that the particle-fiber becomes ductile after the CVD reinforcement.

In summary, we presented a facile route to receive unidirectionally grown and free-standing 1D nanostructures by using uniform nanoparticles. These string-like structures are grouped into forests after fabrication and have a high aspect ratio (length/diameter  $\geq 2500$ ), a uniform profile (diameter of 1.5  $\mu\text{m}$ ), and a relatively strong mechanical strength. CVD is further employed to afford ductility to these brittle nanostructures. Other materials, such as metal and semiconductor nanoparticles, could also be used in our platform. We envision these particle-fibers will offer synergistic, optimized properties of individual 0D elements and, hence, the assembly could operate on larger length scales that allow electrical, optical, or fluidic addressability and interrogation.

## Experimental

**Fabrication:** The particle-fibers are produced by a unidirectional freezing of an aqueous solution of polystyrene (PS) nanoparticles. Typically, the solution is prepared by diluting polystyrene nanoparticles (particle diameter: 80 nm, 10 wt%, Duke Scientific Co.) to 1.0 wt% in distilled water, followed by sonicating for 5 min. The resulting solution is then poured into a cold finger or cylinder (height: 0.5 cm, inner diameter: 1.5 cm) surrounded by a thick wall of Teflon with a stainless steel plate as the bottom. To perform the unidirectional freezing, only the bottom part of the finger is allowed to be immersed in an ethyl alcohol bath, with the top surface exposed to air. The alcohol bath is then cooled to  $-30^\circ\text{C}$  and the whole solution frozen at a freezing rate of  $25.0\ \mu\text{m}\ \text{s}^{-1}$ . Then, the frozen sample is placed in a vacuum vessel and freeze-dried for 24 h to remove the ice.

**Mechanical Strength:** Indentations are performed on two thin films. One film is obtained by spin-coating a 1% PS in chloroform and the other is formed by drop-casting an aqueous suspension (1%) of nanoparticles of PS. In both experiments, glass is used as the substrate and films are allowed to dry under a stream of nitrogen. Subsequently, indentation is performed by using a nanoindenter (Hysteron Bio-Ubi). Quasistatic "trapezoidal" load function tests are performed, with loading 5 s, holding 2 s, and unloading 5 s, and the maximum forces were set as 100  $\mu\text{N}$ . The tip used is a Berkovich tip of a tip radii 70 nm. In this experiment, when the sharp tip is brought into contact with the thin film, the displacement of the tip is recorded along with the applied force.

**Structure Reinforcement:** To strengthen the relief after vacuum drying, (heptadecafluoro-1,1,2,2-tetrahydrodecyl)trichlorosilane (Gelest Inc.) is injected into the vacuum vessel at a pressure of  $1.0 \times 10^{-3}$  Torr and kept sealed for 24 h.

**Imaging:** The microstructure of the samples is characterized by field-emission SEM (Philips) and TEM (JEOL 2010).

## Acknowledgements

The project is financially supported by the Layman Award and the Nebraska Center for Energy Science Research (NCSER). J. Yan is grateful to Prof. J. A. Turner for his generosity in sharing the nanoindenter (assisted by Ben Polly), to Dr. Han Chen and Dr. Xingzhong Li for their assistance with SEM and TEM imaging, and to Ocelio V. Lima for many helpful discussions.

Received: April 24, 2008

Revised: July 25, 2008

Published online: November 12, 2008

- [1] R. A. Metzler, M. Abrecht, R. M. Olabisi, D. Ariosa, C. J. Johnson, B. H. Frazer, S. N. Coppersmith, P. U. P. A. Gilbert, *Phys. Rev. Lett.* **2007**, *98*, 268102.
- [2] H. J. Gao, B. H. Ji, I. L. Jager, E. Arzt, P. Fratzl, *Proc. Natl. Acad. Sci. USA* **2003**, *100*, 5597.
- [3] B. L. Smith, T. E. Schaffer, M. Viani, J. B. Thompson, N. A. Frederick, J. Kindt, A. Belcher, G. D. Stucky, D. E. Morse, P. K. Hansma, *Nature* **1999**, *399*, 761.
- [4] D. P. Burt, N. R. Wilson, J. M. R. Weaver, P. S. Dobson, J. V. Macpherson, *Nano Lett.* **2005**, *5*, 639.
- [5] S. S. Wong, E. Joselevich, A. T. Woolley, C. L. Cheung, C. M. Lieber, *Nature* **1998**, *394*, 52.
- [6] Y. Dzenis, *Science* **2008**, *319*, 419.
- [7] A. Salehi-Khojin, J. J. Stone, W. H. Zhong, *J. Compos. Mater.* **2007**, *41*, 1163.
- [8] J. H. Song, X. D. Wang, J. Liu, H. B. Liu, Y. L. Li, Z. L. Wang, *Nano Lett.* **2008**, *8*, 203.
- [9] Z. L. Wang, *Annu. Rev. Phys. Chem.* **2004**, *55*, 159.
- [10] X. Y. Kong, Z. L. Wang, *Nano Lett.* **2003**, *3*, 1625.
- [11] J. M. Zen, C. T. Hsu, A. S. Kumar, H. J. Lyuu, K. Y. Lin, *Analyst* **2004**, *129*, 841.
- [12] D. Y. Wang, J. S. Li, C. T. Chan, V. Sagueirino-Maceira, L. M. Liz-Marzan, S. Romanov, F. Caruso, *Small* **2005**, *1*, 122.
- [13] G. S. Cheng, M. Moskovits, *Adv. Mater.* **2002**, *14*, 1567.
- [14] H. Yusuf, W. G. Kim, D. H. Lee, M. Aleshyna, A. G. Brolo, M. G. Moffitt, *Langmuir* **2007**, *23*, 5251.
- [15] N. Chandrasekharan, P. V. Kamat, *Nano Lett.* **2001**, *1*, 67.
- [16] Y. H. Cho, G. Cho, J. S. Lee, *Adv. Mater.* **2004**, *16*, 1814.
- [17] Z. Y. Tang, N. A. Kotov, S. Magonov, B. Ozturk, *Nat. Mater.* **2003**, *2*, 413.
- [18] S. Deville, E. Saiz, R. K. Nalla, A. P. Tomsia, *Science* **2006**, *311*, 515.
- [19] M. G. Warner, J. E. Hutchison, *Nat. Mater.* **2003**, *2*, 272.
- [20] O. Cherniavskaya, A. Adzic, C. Knutson, B. J. Gross, L. Zang, R. Liu, D. M. Adams, *Langmuir* **2002**, *18*, 7029.
- [21] S. H. Lee, F. S. Diana, A. Badolato, P. M. Petroff, E. J. Kramer, *J. Appl. Phys.* **2004**, *95*, 5922.
- [22] L. Nagle, D. Ryan, S. Cobbe, D. Fitzmaurice, *Nano Lett.* **2003**, *3*, 51.
- [23] S. Griffith, M. Mondol, D. S. Kong, J. M. Jacobson, *J. Vac. Sci. Technol. B* **2002**, *20*, 2768.
- [24] F. Hua, J. Shi, Y. Lvov, T. Cui, *Nano Lett.* **2002**, *2*, 1219.
- [25] J. X. Huang, F. Kim, A. R. Tao, S. Connor, P. D. Yang, *Nat. Mater.* **2005**, *4*, 896.
- [26] F. Li, X. Badel, J. Linnros, J. B. Wiley, *J. Am. Chem. Soc.* **2005**, *127*, 3268.
- [27] J. H. Moon, S. Kim, G. R. Yi, Y. H. Lee, S. M. Yang, *Langmuir* **2004**, *20*, 2033.
- [28] G. Braun, I. Pavel, A. R. Morrill, D. S. Seferos, G. C. Bazan, N. O. Reich, M. Moskovits, *J. Am. Chem. Soc.* **2007**, *129*, 7760.
- [29] L. J. Brickweg, B. R. Floryancic, E. D. Sapper, R. H. Fernando, *J. Coat. Technol. Res.* **2007**, *4*, 107.
- [30] W. Mahler, M. F. Bechtold, *Nature* **1980**, *285*, 27.
- [31] T. Maki, T. Kokubo, S. Sakka, *Bull. Inst. Chem. Res. Kyoto Univ.* **1986**, *64*, 292.
- [32] T. R. Carale, D. Blankschtein, *J. Phys. Chem.* **1992**, *96*, 459.
- [33] F. De Jaeghere, E. Allemann, J. Feijen, T. Kissel, E. Doelker, R. Gurny, *Pharm. Dev. Technol.* **2000**, *5*, 473.
- [34] Z. P. Zhang, H. D. Yu, Y. B. Wang, M. Y. Han, *Nanotechnology* **2006**, *17*, 2994.
- [35] a) H. F. Zhang, I. Hussain, M. Brust, M. F. Butler, S. P. Rannard, A. I. Cooper, *Nat. Mater.* **2005**, *4*, 787. b) Attempted experiment to use silica nanoparticles as an alternative for the particle-fiber is not successful. Resulting structure shows a plate-like packing.
- [36] K. Walton, *J. Mech. Phys. Solids* **1987**, *35*, 213.
- [37] H. C. Hamaker, *Physica* **1937**, *4*, 1058.
- [38] J. Israelachvili, *Intermolecular and surface forces*, Academic Press, New York **1992**.
- [39] S. P. Timoshenko, J. M. Gere, *Theory of Elastic Stability*, McGraw-Hill, New York **1961**.

[40] J. M. Gere, *Mechanics of Materials*, 5th ed., Brooks/Cole, Pacific Grove, CA 2001.

[41] a) Stacked nanoparticles can be treated as many springs linked in serial. Inside each spring, the stress is distributed through the effective mass along each section of the fiber. Therefore, for the  $i$ -th spring, the effective modulus is linearly proportional to the effective cross-sectional area,  $A$ , and the original modulus of the polymer ( $E_0$ ), or

$$E_i = E_0 \frac{A_i}{A_0} \quad (4)$$

When all of these springs are linked in serial, the final modulus ( $E$ ) will

then be

$$\frac{m}{E} = \sum_{i=1}^n \frac{1}{E_i} \quad (5)$$

The estimated modulus for our fiber is then  $0.606E_0$  and  $l_{cr}$  is 6.4 mm. b) In Ref. 36, we take the confined pressure of 140 MPa to calculate the effective modulus of the fiber, which is 30 MPa and the resulting  $l_{cr}$  is 1.6 mm.

[42] H. J. Lin, J. S. Yang, L. Tan, J. Xu, Z. Li, *J. Phys. Chem. C* **2007**, *111*, 13348.